02,05

Effect of ε-Fe_2O_3 on the superconducting properties of YBCO

© S.V. Semenov[1], D.M. Gokhfeld[1], M.I. Petrov[1], T.D. Balaev[1,2], M.S. Molokeev[1,2], I.V. Nemtsev[1,2], V.L. Kirillov[3], O.N. Martyanov[3]

[1] Kirensky Institute of Physics, Federal Research Center KSC SB, Russian Academy of Sciences, Krasnoyarsk, Russia
[2] Siberian Federal University, Krasnoyarsk, Russia
[3] Boreskov Institute of Catalysis, Siberian Branch of RAS, Novosibirsk, Russia

E-mail: gokhfeld@iph.krasn.ru

Received October 24, 2024
Revised November 15, 2024
Accepted November 16, 2024

The additives of ultra-small ε-Fe_2O_3 nanoparticles affect on the superconducting properties of the high-temperature superconductor $YBa_2Cu_3O_{7-d}$ (YBCO). It has been found that such additives can lead to an increase in the critical current density only without annealing or with short-term annealing during the preparation of YBCO + ε-Fe_2O_3 samples. Prolonged annealing at a temperature of 930°C, which is common for solid-phase synthesis, leads to a significant suppression of the superconducting properties on the surface of the granules.

Keywords: type II superconductors, critical current, spinning, magnetic nanoparticles, magnetic hysteresis.

DOI: 10.61011/PSS.2024.12.60207.277

1. Introduction

One of the most important problems on the way of superconductor introduction into machines and instruments is to increase their critical current density j_c at a process-relevant nitrogen boiling temperature of 77.4 K. Solution of this problem requires controlled creating of pinning centers in a superconducting material. The main methods to create pinning centers are irradiation and introduction of nanoparticle additives. The most effective magnetic flux pinning occurs on magnetic particles introduced into a superconductor. In this case, energy of interaction with the magnetic moment of a particle is added to a normal (non-magnetic) part of interaction between a magnetic vortex with a defect [1–4]. However, it was found that introduction of magnetic particles into superconducting samples often (usually in high concentrations) leads to suppression of critical temperature, see, for example, [5]. This problem may be overcome by placing magnetic nanoparticles on the superconductor surface, rather than inside the superconductor. Such placement of nanoparticles is achieved by means of surface decoration of superconducting films [6–8]. The same effect of increasing intragranular critical current density is achieved by placing magnetic nanoparticles on the surface of superconducting granules [9,10].

The $YBa_2Cu_3O_{7-d}$ superconductor with the critical temperature of $T_c \approx 92$ K may be used in various devices at the nitrogen boiling temperature of 77.4 K. However, such applications are limited to low critical current densities at this temperature. Improvement of transport properties of YBCO in the nitrogen temperatures is a particularly important task. However, creation of composites from YBCO and many types of nanoparticles is difficult due to high reactivity of components and potential undesirable reactions between them. Therefore, important problems include selection of the optimum types and concentrations of nanoparticles, and the development of techniques for synthesizing composites from YBCO and nanoparticles [11]. Previous studies reported that j_c of YBCO increased when the α-Fe_2O_3 (hematite) [12,13] and Fe_3O_4 (magnetite) nanoparticles are added [14]. The sizes of the introduced magnetic particles were 10−100 nm.

ε-Fe_2O_3 is one of the possible candidates for introduction into YBCO. This rare modification of iron oxide is implemented in the form of nanoparticles with sizes up to 10 nanometers [15] and remains stable up to 900°C in the SiO_2 matrix [16]. Effect of such ultra-small iron oxide nanoparticles on the YBCO properties has not been studied earlier. In previous studies of pinning modification in HTSC using magnetic nanoparticles, the best results were achieved at the nanoparticle concentration below 2 wt.% [12–14,17–19]. This article provides the materials study results obtained by adding the ε-Fe_2O_3 nanoparticles to YBCO with concentrations up to 7.41 wt.%.

2. Experiment

$YBa_2Cu_3O_{7-d}$ was synthesized using the standard solid-phase synthesis from Y_2O_3, $BaCO_3$ and CuO powders. ε-Fe_2O_3 nanoparticles were prepared at the Institute of Catalysis, Siberian Branch, RAS, using the technique described in [20].

The samples were prepared by adding alcohol nanoparticle suspension to alcohol-dispersed YBCO powder. Then

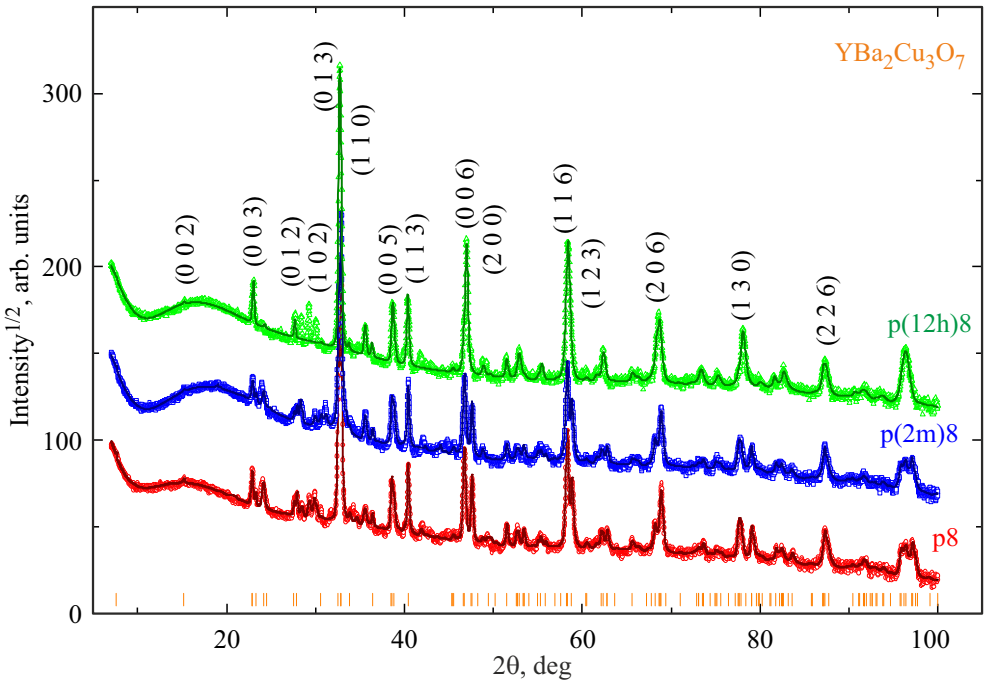

Figure 1. X-ray diffraction analysis od samples (p8, p(2m)8, p(12h)8). Values for different samples are shifted on the y axis. Main reflexes of YBCO are denoted.

Table 1. Ratio of the weight of ε-Fe_2O_3 nanoparticles to weight of m_ε/m_{YBCO} superconductor and the nanoparticle concentration x in the samples

	p0	p01	p03	p07	p1	p2	p4	p8
m_ε/m_{YBCO}	0	0.001	0.003	0.007	0.01	0.02	0.04	0.08
x, wt.%	0	0.1	0.299	0.695	0.990	1.96	3.85	7.41

alcohol was evaporated with mild heating on a hot plate. Stirring was used during all steps. Dry precipitate was triturated thoroughly in a mortar and compacted hydrostatically (≈ 100 MPa). A series of samples with various nanoparticle concentrations from 0 tp 7.41 wt% was prepared. Compacted powder blanks are hard enough and may be machined without pre-annealing. Samples cut from these blanks are denoted as p0, p01, p03, p07, p1, p2, p4, p8 (Table 1).

The compacted blanks were used to prepare another two series of annealed samples, in addition to the first series without annealing. Fast annealing was used to prepare the second series [21]. Compacted samples were placed for 2 minutes into an oven heated up to 930°C. Then the samples were moved to an oven heated up to 400°C and held at this temperature during 10 hours. Samples in this series were denoted as p(2m)0, p(2m)01, p(2m)03, etc.

For the third series, prolonged annealing of samples was performed as for the normal solid-phase synthesis. The compacted samples were placed into an oven heated up to 930°C and annealed at this temperature during 12 hours. Samples in this series were denoted as p(12h)0, p(12h)01, p(12h)03, etc.

Samples were characterized using the X-ray diffraction analysis (Haoyuan DX-2700BH powder diffraction system) and scanning electron microscopy (Hitachi TM4000Plus scanning electron microscope). Distribution of chemical elements on the surface of the samples was determined using the Bruker XFlash 630Hc energy-dispersive spectrometer. magnetization was measured using the LakeShore VSM 8604 vibration magnetometer.

3. Results

Figure 1 shows X-ray diagrams of samples p8, p(2m)8 and p(12h)8. Rietveld analysis shows that the proportion of the YBCO phase decreases during fast annealing, but increases during prolonged annealing (Table 2). The absence of the ε-Fe_2O_3 peaks is attributable to an ultra-small size of iron oxide particles leading to broadening of the corresponding peaks that are recorded against the background of other crystalline phases. New phases are formed during the fast annealing and impurity phases are reduced during the prolonged annealing (Table 2). During the prolonged annealing, the ε-Fe_2O_3 nanoparticles interact with YBCO forming $BaFe_2O_4$. During the prolonged annealing, iron atoms are probably arranged in a YBCO lattice [22,23].

Figure 2 shows the image of sample p(2m)4 recorded using the scanning electron microscopy method. Granules forming the sample have a mean size of about

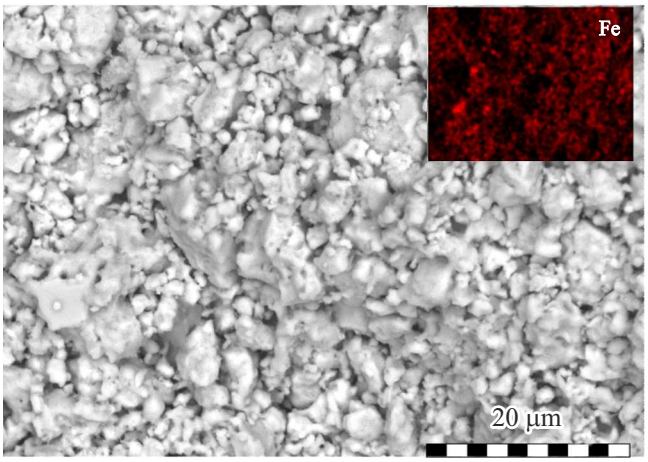

Figure 2. Scanning electron microscopy of sample p(2m)4. The inset shows Fe atom distribution on the granule surfaces.

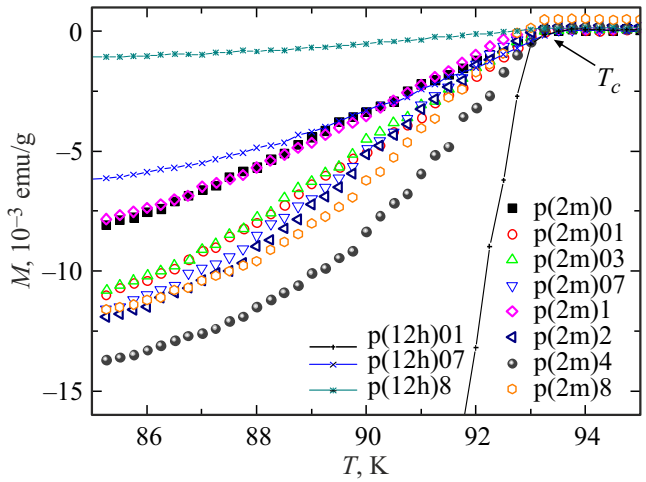

Figure 3. Temperature dependences of magnetization measured after zero-field cooling (ZFC).

2 micrometers. The inset in Figure 2 shows a relatively uniform distribution of iron on the granule surfaces. The energy-dispersive spectroscopy shows that almost uniform distribution of the ε-Fe_2O_3 nanoparticles around granules is achieved during preparation of the samples.

Superconducting transition temperature T_c was determined by the inflection point on the temperature dependence of magnetization (as shown by the arrow in Figure 3) and appeared to be the same for all samples, $T_c = 92.6$ K. Thus, for the used sample preparation method, nanoparticles didn't affect the critical temperature of the whole superconductor. Figure 3 shows the temperature dependences of magnetization $M(T)$ of samples p(2m)0−p(2m)8, p(12h)01, p(12h)07 and p(12h)8. For sample series p(2m)0−p(2m)8, diamagnetic signal increases when nanoparticles are added, with sample p(2m)4 having the maximum diamagnetic signal. For sample series p(12h)0−p(12h)8, sample p(12h)0 has the maximum

Table 2. Concentrations of various phases in the samples according to the XRD data

	p8	p(2m)8	p(12h)8
$YBa_2Cu_3O_7$	80.11	76.55	91.68
CuO	5.85	7.39	8.32
$BaCuO_2$	4.41	–	–
Y_2O_3	2.88	–	–
Y_2CuO_4	6.75	5.29	–
$BaFe_2O_4$	–	3.80	–
$YBa_6Cu_3O_{11}$	–	6.97	–

Table 3. Maximum values of ΔM for samples from different series

	p0	p(2m)0	p(12h)0	p4	p(2m)4	p(12h)4
ΔM (emu/g)	0.397	0.213	0.645	0.516	0.382	0.015

diamagnetic signal, the diamagnetic signal decreases as the nanoparticle concentration increases.

Figure 4, *a* shows the magnetic hysteresis loops of samples p(2m)0−p(2m)8 and p(12h)8 at 77 K. ΔM, difference between the upper and lower sections of the loop for sample p(2m)4 is larger than for other samples in series p(2m)0−p(2m)8. Maximum values of ΔM for YBCO and YBCO with 4 wt.% of ε-Fe_2O_3 from different series are listed in Table 3. Figure 4, *b* shows field dependences of magnetization of samples p8, p(2m)8 and p(12h)8 at 100 K. Magnetic hysteresis differs considerably for samples from different series despite the same initial nanoparticle concentrations. Difference of the magnetic hysteresis loops measured above the superconducting transition temperature (Figure 4, *b*) indicates that heating of YBCO + ε-Fe_2O_3 up to 930°C leads to the transformation of the ε-Fe_2O_3 phase.

Figure 5 shows the values of ΔM in the magnetization peak point normalized to ΔM of the samples with $x = 0$ in each of the series. The obtained data makes it possible to divide the effect of annealing and nanoparticle addition by the YBCO properties. Initial sample p0 contained just about 80 wt.% of the YBCO phase and unreacted initial components. After the fast annealing, new phases were formed and the proportion of the YBCO phase reduced to 77 wt.%. After the prolonged annealing, the proportion of the YBCO phase increased up to 92 wt.%, and the granules sizes also increased. This led to large ΔM for p(12h)0 compared with p0 and p(2m)0.

Addition of nanoparticles led to the increase in ΔM for the series of sample p01−p8 and p(2m)01−p(2m)8 (Figure 5). Sample p(2m)4 has the highest normalized ΔM among all studied samples. For a series of samples p(12h)01−p(12h)8, increase in the concentration of initial nanoparticles leads to a significant increase in ΔM. Iron atoms in this series of samples are probably incorporated into the YBCO lattice in the surface granule layer. As a

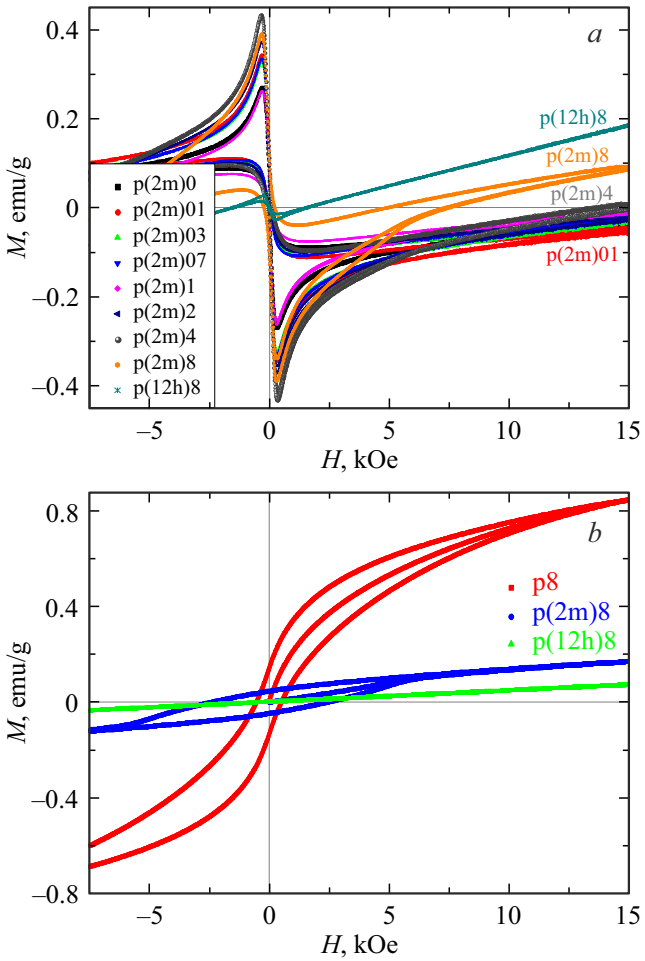

Figure 4. Magnetization hysteresis loop at 77 K (a) and 100 K (b).

result of Fe incorporation, the critical superconductor temperature in this surface layer decreases considerably [22,23] and becomes lower than 77 K. In the central granular area, T_c is still equal to 92.6 K, which can be seen on curves $M(T)$. The higher the initial nanoparticle concentration is, the thicker the layer with suppressed superconductivity is.

ΔM depends on the critical current density, current circulation scale and proportion of the superconducting phase. Variation ofΔM in different annealing conditions is associated with variation of the proportion of the superconducting YBCO phase. To take into account the contribution of the superconducting granules within one series, values of magnetization or the same samples with the same magnetic history at 100 K were subtracted from the magnetization at 77 K (Figure 4, b). Thus, the ferromagnetic hysteresis contribution was removed.

For polycrystalline superconductors, magnetic hysteresis was defined by intergranular currents [24]. Intragranular critical current density was calculated using equation $j_c(H) = 3\Delta M(H)/D$, where D is the mean granule size. The mean granule size estimated from microphotographs and from the magnetic loop asymmetry [25] was 2.2 μm for samples p0–p8 and p(2m)0–p(2m)8.

The estimated dependences $j_c(H)$ of samples p(2m)0–p(2m)8 are shown in Figure 6. When nanoparticles are added, the critical current density increases, and the highest value $j_c = 3.01 \cdot 10^5$ A/cm^2 is achieved in sample p(2m)4. The critical current density in this sample is 74% higher than in p(2m)0. In series p0–p8, sample p2 has the maximum critical current density $j_c = 4.09 \cdot 10^5$ A/cm^2, which is 24% higher than in p0.

Let's compare the obtained values with the data in [26] that studied the REBCO tapes irradiated by iron ions. Critical current density in the irradiated tapes increased up to $1.3 \cdot 10^6$ A/cm^2 at $T = 77$ K. In the studied samples, values of j_c are lower by 70%. The root cause behind the low

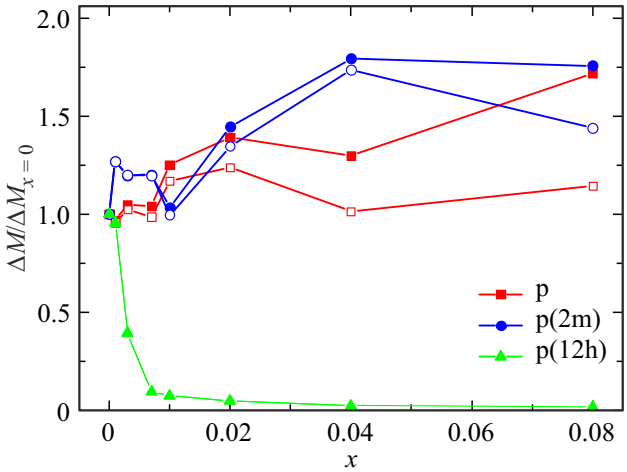

Figure 5. Normalized values of ΔM for all samples at 77 K. Filled symbols — values of ΔM of the experimental loops. Empty symbols — values of ΔM for superconducting granules (after deduction of the ferromagnetic contribution).

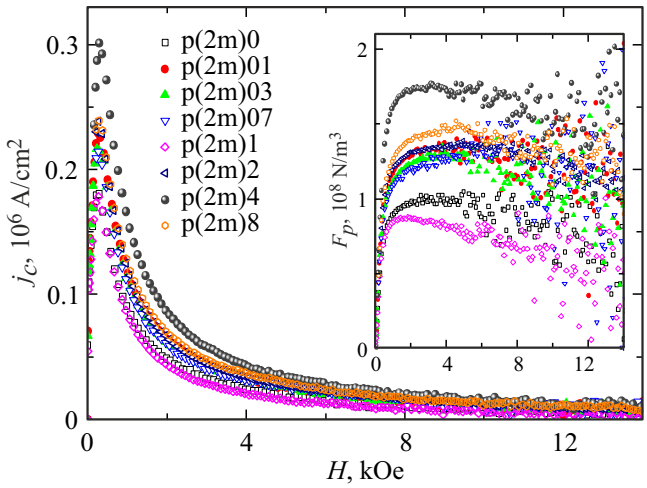

Figure 6. Intragranular critical current density for p(2m)0–p(2m)8 at 77 K. Dependences of pinning force on magnetic field are shown in the inset.

values of j_c in the studied materials is inadequate quality of the initial YBCO powder containing nonsuperconducting phases. Optimization of synthesis and pure precursors will improve material properties.

Field dependences of the pinning force $F_p = \mu_0 H j_c(H)$ are shown in the inset in Figure 6. Irreversibility fields H_{irr} above which $F_p = 0$ were not achieved in this study, i. e. exceed 15 kOe at $T = 77$ K. However, different maximum positions of $F_p(H)$ indicate that nanoparticles affect the value of H_{irr}.

The identified increase in the critical current density, when ε-Fe_2O_3 is added, is associated with pinning strengthening due to the interaction of the Abrikosov vortices passing through the superconductor granules with magnetic moments of nanoparticles on the granules surfaces. Pinning may increase due to the matching effect [27]. Pinning increases due to this effect, if the mean distance between the pinning centers corresponds to the distance between the Abrikosov vortices that is approximately equal to λ, depth of magnetic field penetration into the superconductor.

Let's consider the potential implementation of the matching effect in the studied samples. For YBCO at $T = 77$ K, $\lambda \approx 300$ nm. In samples p2, p4, up to 10^6 nanoparticles fall within one granule. In case of uniform distribution, the mean distance between the nanoparticles is ~ 10 nm. This much lower than the value expected for the matching effect. However, it is hard to provide uniform coating of the granules surfaces with single nanoparticles through the sample preparation method used. In our opinion, the studied samples have clusters containing ~ 100 nanoparticles on the granule surfaces. The mean distance between such clusters corresponds to the matching effect. With further increase in the nanoparticle concentration, unwanted superconductivity suppression effects may occur leading to reduction of ΔM.

4. Conclusion

It was found that addition of the ε-Fe_2O_3 nanoparticles modifies magnetic properties of the polycrystalline YBCO. Magnetic nanoparticles on the granule surfaces increase the magnetic flux pinning and improve the intragranular current density. Nanoparticle concentration, annealing temperature and duration play an important role in the improvement of the transport properties. Maximum increase in the critical current density (up to 74%) is achieved through addition of 2−4 wt.% of nanoparticles and the absence of prolonged annealing of samples.

Acknowledgments

Scanning electron microscopy, X-ray diffraction analysis and magnetic measurements were carried out on the equipment provided by Krasnoyarsk Regional Center of Research Equipment of Federal Research Center „Krasnoyarsk Science Center SB RAS". The authors are grateful to D.A. Balaev and Yu.S. Gokhfeld for fruitful discussion of findings.

Funding

This study was supported by grant provided by the Russian Science Foundation No. 24-22-00053, https://rscf.ru/project/24-22-00053/

Conflict of interest

The authors declare no conflict of interest.

References

[1] A. Snezhko, T. Prozorov, R. Prozorov. Phys. Rev. B **71**, 024527 (2005).
[2] V.A. Kashurnikov, A.N. Maximova, I.A. Rudnev. FTT **56**, 861 (2014). (in Russian).
[3] J. Huang, H. Wang, Supercond. Sci. Technol. **30**, 114004 (2017).
[4] A.N. Maximova, I.A. Rudnev, V.A. Kashurnikov, A.N. Moroz. FTT **65**, 531 (2023). (in Russian).
[5] N. Novosel, E. Babić. Phys. C Supercond. **493**, 119 (2013).
[6] T. Aytug, M. Paranthaman, K.J. Leonard, K. Kim, A.O. Ijaduola, Y. Zhang, E. Tuncer, J.R. Thompson, D.K. Christen. J. Appl. Phys. **104**, 043906 (2008).
[7] A.K. Jha, N. Khare, R. Pinto. J. Appl. Phys. **110**, (2011).
[8] A. Palau, F. Valles, V. Rouco, M. Coll, Z. Li, C. Pop, B. Mundet, J. Gazquez, R. Guzman, J. Gutierrez, et al. Supercond. Sci. Technol. **31**, 034004 (2018).
[9] E. Altin, D.M. Gokhfeld, S.V. Komogortsev, S. Altin, M.E. Yakinci. J. Mater. Sci. Mater. Electron. **24**, 1341 (2013).
[10] A.A. Lepeshev, G.S. Patrin, G.Y. Yurkin, A.D. Vasiliev, I.V. Nemtsev, D.M. Gokhfeld, A.D. Balaev, V.G. Demin, E.P. Bachurina, I.V. Karpov, A.V. Ushakov, L.Yu. Fedorov, L.A. Irtyugo, M.I. Petrov. J. Supercond. Nov. Magn. **31**, *12*, 3841 (2018).
[11] P.E. Kazin, Yu.D. Tretyakov. Uspekhi khimii **72**, 960 (2003). (in Russian).
[12] S.C. Wimbush, J.H. Durrell, R. Bali, R. Yu, H. Wang, S.A. Harrington, J.L. MacManus-Driscoll. IEEE Trans. Appl. Supercond. **19**, 3148 (2009).
[13] J. Wang, C.F. Tsai, Z. Bi, D.G. Naugle, H. Wang. IEEE Trans. Appl. Supercond. **19**, 3503 (2009).
[14] X. Dong, P. An, J. Zhang, H. Zhang, Y. Li, H. Liu, X. Ge, Q. Li. J. Supercond. Nov. Magn. **27**, 693 (2014).
[15] S.S. Yakushkin, A.A. Dubrovskiy, D.A. Balaev, K.A. Shaykhutdinov, G.A. Bukhtiyarova, O.N. Martyanov. J. Appl. Phys. **111**, 044312 (2012).
[16] G.A. Bukhtiyarova, M.A. Shuvaeva, O.A. Bayukov, S.S. Yakushkin, O.N. Martyanov. J. Nanoparticle Res. **13**, 5527 (2011).
[17] A.T. Pham, D.T. Tran, H.H. Pham, N.H. Nam, L.T. Tai, D.H. Tran. Mater. Lett. **298**, 130015 (2021).
[18] R.A. Algarni, Y. Slimani, E. Hannachi, M.A. Almessiere, T.M. Alqahtani, F. Ben Azzouz. J. Mater. Sci. Mater. Electron. **34**, 1 (2023).
[19] M.A. Ali, S.M. Karan, N. Roy, S.S. Banerjee. AIP Adv. **14**, 035110 (2024).

[20] D.A. Balaev,V.L. Kirillov, A.A. Dubrovsky, S.V. Semenov, Yu.V. Knyazev, M.N. Volochaev, O.N. Martianov. Pisma v ZhTF **50**, 16 (2024). (in Russian).
[21] D.A. Balaev, K.A. Shaihutdinov, S.I. Popkov, D.M. Gokhfeld, M.I. Petrov. Supercond. Sci. Technol. **17**, 175 (2004).
[22] P. Pęczkowski, P. Zachariasz, M. Kowalik, W. Tokarz, S.P. Kumar Naik, J. Żukrowski, C. Jastrzębski, L.J. Dadiel, W. Tabiś, Ł. Gondek. J. Eur. Ceram. Soc. **41**, 7085 (2021).
[23] K.S. Pigalsky, A.A. Vishnyov, N.N. Efimov, P.N. Vasiliev, A.V. Shabatin,L.I. Trakhtenberg. ZhETF, **166**, 246 (2024). (in Russian).
[24] D.M. Gokhfeld. J. Supercond. Nov. Magn. **36**, 1089 (2023).
[25] D.M. Gokhfeld. Pisma v ZhTF **45**, 3 (2019). (in Russian).
[26] I.A. Rudnev, A.I. Podlivaev, D.A. Abin, S.V. Pokrovsky, A.S. Starkovsky, R.G. Batulin, P.A. Fedin, K.E. Pryanishnikov, T.V. Kulevoy. FTT **65**, 386 (2023). (in Russian).
[27] L. Opherden, M. Sieger, P. Pahlke, R. Huhne, L. Schultz, A. Meledin, G. Van Tendeloo, R. Nast, B. Holzapfel, M. Bianchetti, J.L. MacManus-Driscoll, J. Hänisch. Sci. Rep. **6**, 1 (2016).

Translated by E.Ilinskaya